

ANALYSIS AND MEASUREMENT OF SCARF-LAP AND STEP-LAP JOINT REPAIR IN COMPOSITE LAMINATES

David H. Mollenhauer*, Brian Fredrickson*, Greg Schoeppner*, Endel V. Iarve**, and Anthony N. Palazotto*** [David H. Mollenhauer]: david.mollenhauer@wpafb.af.mil
 *U.S. Air Force Research Laboratory, **University of Dayton Research Institute, and U.S. Air Force Institute of Technology

Keywords: *Composite, Bonded Repair, Scarf-Lap Joint, Step-Lap Joint, Moiré Interferometry*

1 INTRODUCTION

As composites usage on aircraft increases, the need for viable repair techniques is becoming more urgent. Externally bonded or bolted patches are only suited for lightly loaded structures that are not aerodynamic and/or signature critical. Flush repairs (scarf-lap and step-lap) are necessary to restore original stiffness and nearly original strength, while maintaining outer surface smoothness. A scarf joint repair is described by the removal of the damaged area and the process of tapering or “scarfing” the perimeter of the undamaged portion of the composite. A patch is then cut and scarfed to match the opening and then bonded in place. A step-lap joint is essentially the same with the exception that the scarf is not a simple taper, but a series of steps that form the taper (See Fig.1). Each step is sometimes only as deep as one ply grouping. Both of these repairs are typically expensive and time consuming to accomplish, so a thorough understanding of their behavior is necessary.

This paper will follow from the work of Cook [1] (scarf-lap joints) and Fredrickson [2] (scarf-lap and step-lap joints). In both studies, experimentally obtained, full-field strain distributions were obtained using moiré interferometry. Complimentary models were developed using an in-house developed numerical model [3]. These models attempted to match the actual geometry of the test specimens as closely as possible. However, an exact geometric match was impossible. Recent advances in the modeling method now allow for more exact geometric matches to the test specimens. Both experimental results and new numerical analyses are presented.

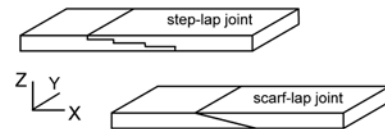


Figure 1: Schematic representation of model scarf-lap and step-lap joints.

2 EXPERIMENTAL PROCEDURE

2.1 Specimen Description

Model scarf-lap and step-lap specimens were manufactured for mechanical testing and testing with moiré interferometry. These were manufactured as panels using IM6/3501-6 with a $[45_2/0_2/-45_2/90_2]_s$ ply stacking sequence. The scarf angle was 4.35 degrees and manufactured on a specialized sanding fixture. The step-lap was cut using a high-precision milling machine equipped with a diamond coated cutting bit. Each step was 2 plies in depth, resulting in 8 steps. Cyanamid FM300M film adhesive was used to bond the specimen panels together. The test specimens were then cut to 25.4 mm in width.

2.2 Moiré Interferometry

Moiré interferometry examinations were made on one of the free-edges of each specimen. The specimens were loaded using a small table-top load frame suitable for interferometric use. Due to the high aspect ratio of the images (length of bondline compared with specimen thickness) and the desire to achieve maximum spatial resolution through the specimen thickness, a data stitching scheme was implemented. In this scheme, the region of interest spanned only a small portion of the bondline at a time. After data was gathered at a given location, the specimen was precisely shifted to examine an overlapping portion of the bondline. Several such

overlap regions were gathered and the final data “stitched” together for comparison with the model data. Figure 2 shows an example of 2 fringe patterns with the overlap regions outlined in red.

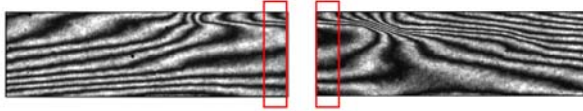


Figure 2: Photo-stitched displacement fringe patterns. Overlapping regions indicated by the red outlines.

3 MODELING

3.1 Previous Efforts

In the previous modeling efforts, a code being developed jointly by the University of Dayton Research Institute and the U.S. Air Force Research Laboratory was used. The code is known as the B-Spline Analysis Method (BSAM). In the original effort, the geometry definitions for were quite basic [2]. They captured only the approximate shape of each type of specimen. In the actual specimens, significant departures from the ideal were present. For the scarf-lap joint, these manifested themselves as departures from flatness of the scarf angle resulting in variation in the bondline thickness (see Fig 3). The step machining process resulted in rounded corners of each step, rather than the precise square steps modeled (see Fig 4).

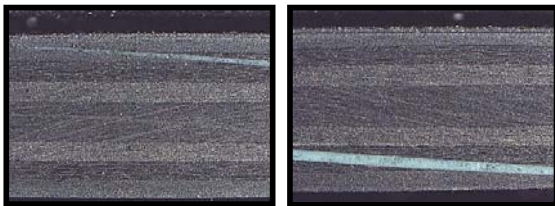


Figure 3: Variation in bondline thickness for the scarf-lap joint. Bondline is in blue.

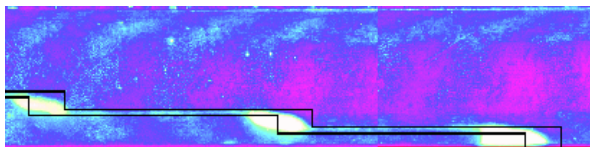


Figure 4: Difference in geometry between modeled scarf-lap (black lines) and actual scarf-lap (white space).

3.2 Specimen Modeling

In a departure from our previous work [2], the scarf and step geometries were precisely matched to the experimental specimens. This was accomplished by first removing the reflective coating from each specimen grating with a cotton swab and polishing compound. Images of the specimens were then obtained using a flat-bed scanner at 126 pixels/mm (see Figure 5). The shapes of the bond-lines were then digitized and input into the BSAM models. Note that in the step-lap joint, the axial locations of the adherends is offset, resulting in rather large resin pockets. Also note that the scarf-lap bondline is significantly thicker towards the right side of the specimen.



Figure 5: Scanned images of the step-lap and scarf-lap joints.

Additionally, the orientation of the step-lap moiré specimen in the loading fixture created a stacking sequence where the 45° and -45° plies angles were reversed. Thus the step-lap specimen was modeled using a stacking sequence of $[-45_2/0_2/+45_2/90_2]_s$ and the scarf-lap modeled using the original stacking sequence of $[+45_2/0_2/-45_2/90_2]_s$. These models were loaded through a constant end displacement that produced an average axial strain equivalent to that recorded in each moiré test.

Previous efforts showed an odd reversal of the ϵ_z strain component occurred in the center of the adhesive line for the scarf-lap joint that was not predicted by the modeling effort. To a lesser degree, this trend was also observed in the step-lap specimen. Because of this observation and a suspicion that the diffraction grating layer may be the cause of the discrepancy, an additional model of the scarf-lap joint with a layer of resin $50 \mu\text{m}$ thick representing the diffraction grating was constructed and results obtained.

For both the step-lap and the 2 scarf-lap models the discretization mesh was more refined in the region of the bonded line and the free edges. Refinement of the mesh in these areas allowed the BSAM code to produce a more accurate strain field prediction in the areas of interest.

4 RESULTS AND DISCUSSION

4.1 Experimental/Analytical Comparison – General Comments

For comparison to moiré data, the strain data on the free-edge of the coupon corresponding to the moiré interferometry field of view was extracted from the full three-dimensional BSAM model results. The data were then interpolated to a data spacing matching the original moiré data of 8680 by 494 for the scarf-lap specimen and 7250 by 460 for the step-lap specimen. The normal strains (ϵ_x , ϵ_z) and the shear strain (γ_{xz}) were then smoothed in precisely the same manner as the moiré data. Smoothing the numerical predictions produces a more consistent comparison between numerical and experimental data.

4.2 Step-lap Joint Comparison

The distribution of axial (ϵ_x) strain is shown for the whole field in Figure 6 and across the line $X=-9.00\text{mm}$ in Figure 7. The X-direction origin of the coordinate system is located at the center of the bondline. Immediately clear in Figure 6 is the character of the step-lap adhesive layer. The large resin pockets stand out in both the experimental and numerical results. The comparison of strain across the whole field of view is quite close. The predicted magnitude of the left-most large peak (at $X=-9.00\text{mm}$) is shown in Figure 7 to be higher and narrower than the moiré results. As the BSAM model contained no representation of the grating, the differences may be a result of strain shielding through the grating.

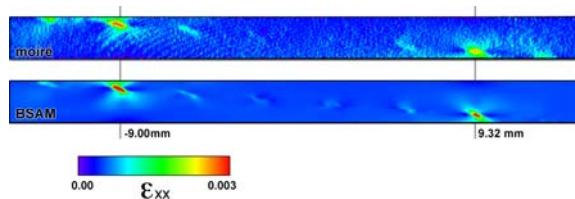


Figure 6: Comparison of the axial (ϵ_x) strain component for the step-lap joint. X-coordinate lines indicate locations of interest.

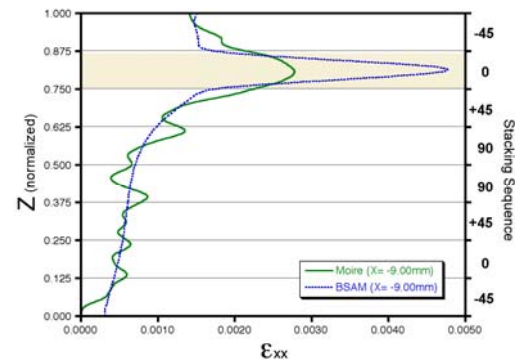


Figure 7: Comparison of the axial (ϵ_x) strain component for the step-lap joint at $X=-9.00\text{mm}$ from the center of the bondline. Shaded (tan) regions indicate the location of the adhesive bondline.

Figures 8 and 9 show the distribution of transverse (ϵ_z) strain across the whole field and along the line $X=-9.00\text{mm}$, respectively. Again, the step-lap adhesive structure is clearly indicated by both sets of data. While generally lower in magnitude, the predicted strains match the trends shown by the measured strains. An example of an exquisite match in the trends can be seen to the left of the $X=-9.00\text{mm}$ line, just above the specimen centerline. The subtle variations in strain in the experimental data are matched precisely (in trend) with the predicted results.

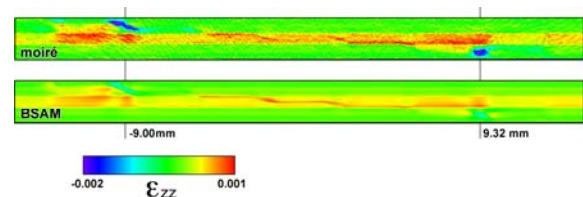


Figure 8: Comparison of the transverse (ϵ_z) strain component for the step-lap joint. X-coordinate lines indicate locations of interest.

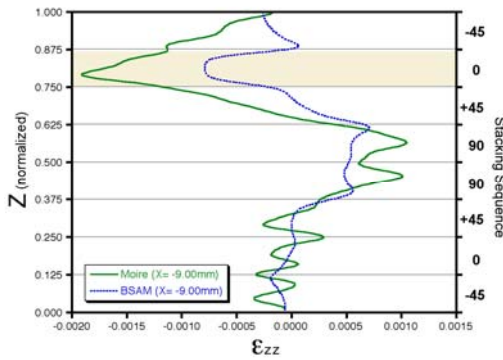


Figure 9: Comparison of the transverse (ϵ_{zz}) strain component for the step-lap joint at $X=-9.00\text{mm}$ from the center of the bondline. Shaded (tan) regions indicate the location of the adhesive bondline.

Finally, the shear (γ_{xz}) strain component is shown across the whole field of view in Figure 10 and along the lines $X=-9.00\text{mm}$ and $X=9.32\text{mm}$ in Figures 11 and 12, respectively. The predicted magnitudes and trends match very closely with the measured data across the whole specimen. The largest shear strain peak occurs at $X=-9.00\text{mm}$ and is matched by the prediction well (see Figure 11). The peak is larger at this location than at the $X=9.32\text{mm}$ location due to the shear strain of the parent adherends enhancing the strain along the top half of the specimen and retarding the strain along the bottom half of the specimen.

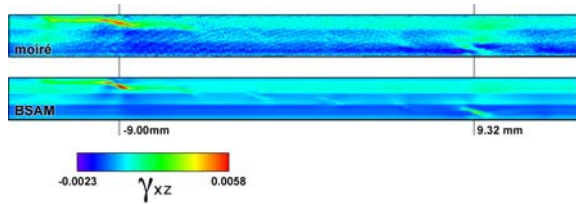


Figure 10: Comparison of the shear (γ_{xz}) strain component for the step-lap joint. X-coordinate lines indicate locations of interest.

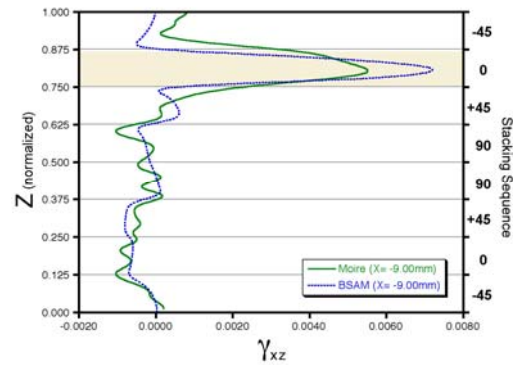


Figure 11: Comparison of the shear (γ_{xz}) strain component for the step-lap joint at $X=-9.00\text{mm}$ from the center of the bondline. Shaded (tan) regions indicate the location of the adhesive bondline.

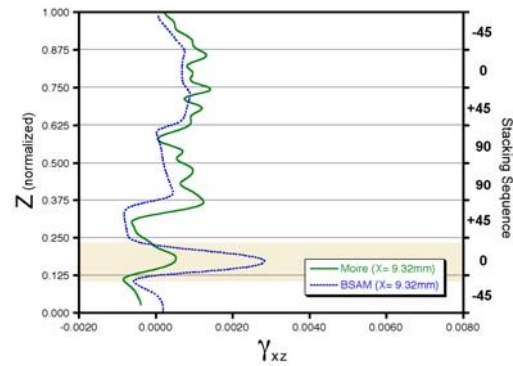


Figure 12: Comparison of the shear (γ_{xz}) strain component for the step-lap joint at $X=9.32\text{mm}$ from the center of the bondline. Shaded (tan) regions indicate the location of the adhesive bondline.

4.3 Scarf-Lap Joint Comparison

The distribution of axial (ϵ_x) strain is shown for the whole field in Figure 13 and across the line $X=9.00\text{mm}$ in Figure 14. Again, the X-direction origin of the coordinate system is located at the center of the bondline. Unlike the step-lap joint, evidence of the scarf bondline is primarily evident at the right of the specimen. This is likely due to the variation of the bondline thickness as shown in Figure 5 where the bondline is clearly thicker toward the right side of the specimen. Predicted magnitudes are generally very close to the moiré data. Figure 14 shows that the addition of the grating layer to the model improved the match, both in magnitude and breadth, in the region of the bondline, supporting the supposition indicated above for the step-lap axial strain.

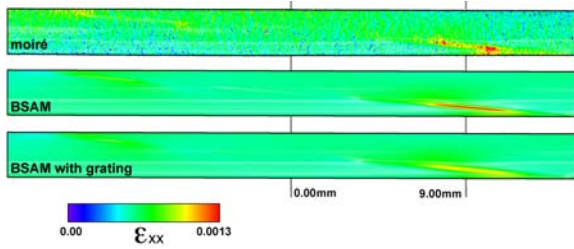


Figure 13: Comparison of the axial (ϵ_x) strain component for the scarf-lap joint. X-coordinate lines indicate locations of interest.

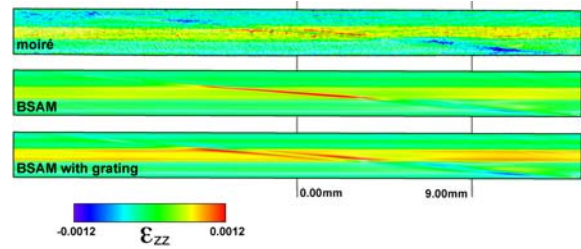


Figure 15: Comparison of the transverse (ϵ_z) strain component for the scarf-lap joint. X-coordinate lines indicate locations of interest.

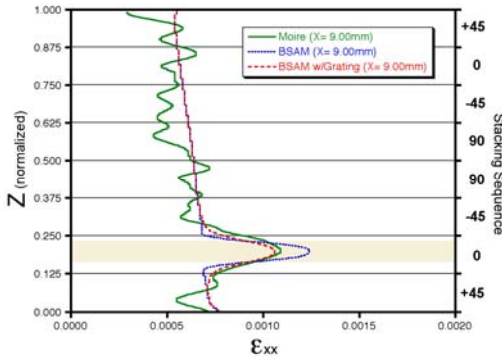


Figure 14: Comparison of the axial (ϵ_x) strain component for the scarf-lap joint at $X=9.00\text{mm}$ from the center of the bondline. Shaded (tan) regions indicate the location of the adhesive bondline.

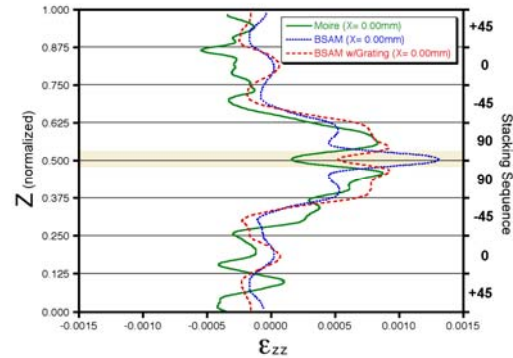


Figure 16: Comparison of the transverse (ϵ_z) strain component for the scarf-lap joint at $X=0.00\text{mm}$ from the center of the bondline. Shaded (tan) regions indicate the location of the adhesive bondline.

Figures 15 and 16 show the distribution of transverse (ϵ_z) strain across the whole field and along the line $X=0.00\text{mm}$, respectively. The scarf bondline is again more evident toward the right side of the specimen than at the left. However, the primary evidence of the bondline occurs in the center region of the specimen where high overall transverse strain exists in the 90° plies. As noted above and in [2], an odd reversal in strain occurs across the bondline in the experimental data (see Figure 16). This is not represented by the BSAM model without the grating. However, the BSAM model with the representative grating layer exactly matches this observed trend and, in general, brings the prediction closer to the experimental data across the whole field of view.

The shear (γ_{xz}) strain component is shown across the whole field of view in Figure 17 and along the line $X=9.00\text{mm}$ in Figure 18. The scarf bondline is evident across the whole field with the primary peak occurring where the bondline is thickest and the adherend free-edge shear enhances the bondline shear. The overall predicted magnitudes match quite well with the experimental data. The addition of the grating resin layer over the face of the model improves the prediction remarkably as shown in Figure 17 and, especially, in Figure 18.

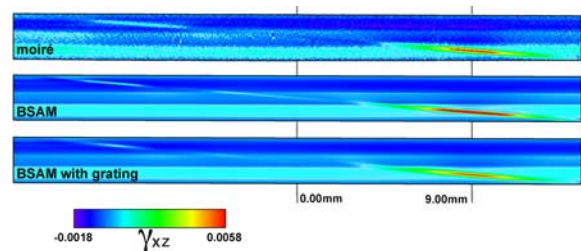


Figure 17: Comparison of the shear (γ_{xz}) strain component for the scarf-lap joint. X-coordinate lines indicate locations of interest.

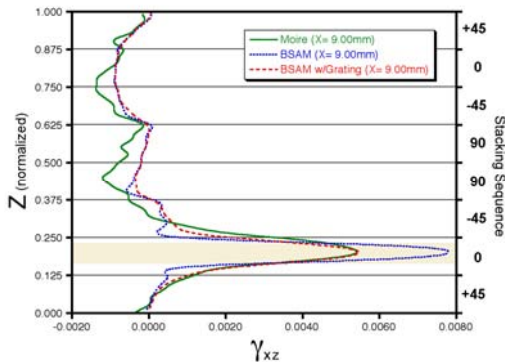


Figure 18: Comparison of the shear (γ_{xz}) strain component for the scarf-lap joint at $X=9.00\text{mm}$ from the center of the bondline. Shaded (tan) regions indicate the location of the adhesive bondline.

4.4 Discussion

There are a few main points of discussion resulting from this current research. The first is that the results from a modeling effort are only as good as the input to the model. Namely, the more precise representation of the scarf-lap and step-lap bondline geometries resulted in close agreement with experiment. This is true in locations of high strain where the models in [2] failed to produce such close agreement. Further improvements were shown by the addition of a resin layer representing the grating. The grating is a real feature of the test specimens and the results, especially the transverse strain component (see Figure 16), are significantly closer to the experimental data.

The second point is that a full-field experimental method is an invaluable tool in validation of a modeling effort. Subtle details in a model are often overlooked as some sort of numerical effect or error in the modeling method. With a suitable experimental method, moiré interferometry in this case, many of these subtle details emerge as true behavior. With sufficiently refined input data, modern modeling methods are capable of capturing exquisitely fine details.

The final point of discussion concerns the quality of load transfer of the two flush repair methods. It appears that the scarf repair is superior in some respects. Generally, the peak values of the two normal components of strain are lower for the scarf-lap joint than for the step-lap joint. The peak shear strains are equivalent for both specimens. High peak values occur in the large resin pockets of the step-lap specimen. These peaks may be

significantly reduced if the axial alignment is better controlled. The peak values of the scarf repair coupon may also be reduced if the bondline is more uniform and thinner.

With the enhanced confidence in the available modeling tool, BSAM in this research effort, these suppositions can be explored in the virtual world and an optimized configuration determined. However, should the modeling effort depart significantly from the validated situations (i.e. material nonlinearities, geometric nonlinearities, viscoelasticity, residual stresses), further experimentation will be necessary to validate these new models.

5 CONCLUSION

An experimental/numerical investigation of step-lap and scarf-lap repair schemes in composite materials was conducted. It is a follow-on from previous efforts where the modeling effort, although sophisticated in many ways, lacked the geometric detail necessary to completely capture the strain distributions measured with the full-field experimental method, moiré interferometry. The current research effort more precisely matched the test specimen geometries by digitizing the actual bondlines and applying the resulting geometry to a numerical model. The modeling tool, a fully 3-D method known as BSAM, produced strain distributions that closely matched the moiré interferometric strain data for both specimens. A further refinement to the scarf-lap model consisted of the addition of a thin resin layer, mimicking the moiré diffraction grating, over the region of interest. The results for this case were even closer to those observed in the experiment.

Through this detailed modeling and experimental effort, great confidence in the linear-elastic modeling method, BSAM, was gained for these joint configurations. Further efforts will focus on optimizing the joint geometries and providing guidance to the composite repair community.

REFERENCES

- [1] Cook, B., Schoeppner, G., and Palazotto, A., "Thermal and Mechanical Strain Fields in Composite Scarf Joints," *Proceedings of the American Society for Composites 20th Technical Conference*, Drexel University, Philadelphia, PA, paper number 59, 7-9 September, (2005).

- [2] Fredrickson, B., Mollenhauer, D., Schoeppner, G., and Palazotto, A., "Measurement and Prediction of Strain Fields in Composite Scarf and Step-lap Joints," *Proceedings of the American Society for Composites 21st Technical Conference*, University of Michigan-Dearborn, Dearborn, MI, paper number 59, 17-20 September, (2006).
- [3] Iarve, E., "Spline Variational Three Dimensional Stress Analysis of Laminated Composite Plates with Open Holes," *International Journal of Solids and Structures*, Vol. 33, No. 14, pp. 2095-2118, (1996).